

A Visual-Inertial Motion Prior SLAM for Dynamic Environments

Weilong Sun¹, Yumin Zhang^{2*} and Boren Wei²

Abstract—The Visual-Inertial Simultaneous Localization and Mapping (VI-SLAM) algorithms which are mostly based on static assumption are widely used in fields such as robotics, UAVs, VR, and autonomous driving. To overcome the localization risks caused by dynamic landmarks in most VI-SLAM systems, a robust visual-inertial motion prior SLAM system, named (*IDY-VINS*), is proposed in this paper which effectively handles dynamic landmarks using inertial motion prior for dynamic environments to varying degrees. Specifically, potential dynamic landmarks are preprocessed during the feature tracking phase by the probabilistic model of landmarks' minimum projection errors which are obtained from inertial motion prior and epipolar constraint. Subsequently, a bundle adjustment (BA) residual is proposed considering the minimum projection error prior for dynamic candidate landmarks. This residual is integrated into a sliding window based nonlinear optimization process to estimate camera poses, IMU states and landmark positions while minimizing the impact of dynamic candidate landmarks that deviate from the motion prior. Finally, experimental results demonstrate that our proposed system outperforms state-of-the-art methods in terms of localization accuracy and time cost by robustly mitigating the influence of dynamic landmarks.

I. INTRODUCTION

In environments without satellite positioning, V-SLAM obtains information of the surrounding environment through visual sensors to solve its own motion. It has the advantages of low cost, high precision in trajectory estimation within small areas, no need for any environmental prior, and rich applicable scenarios. However, visual-only sensor is easily affected by external environmental and motion factors, such as dynamic landmarks, the lack of texture, lighting conditions, motion blur, and few common field of view (FOV) [1]. Therefore, an inertial measurement unit (IMU), which can provide relatively accurate pose estimation information without being affected by the environment in a short period of time, can be integrated to compensate for the deficiencies of visual-only sensor [2].

However, the assumption of static landmarks in visual-related SLAM still makes it has hidden localization risk in environments with dynamic landmarks [3]. The dynamic landmarks will affect the accuracy of visual positioning, and in extreme cases, they will lead to rapid deterioration of positioning.

In recent years, research on visual-related SLAM in dynamic environments has gradually become a focus. Most

studies seek solutions through deep learning methods such as semantic recognition [4], [5] while some studies use geometric methods [6], [7]. However, deep learning methods are always limited by scenes and training processes while geometric methods always have low-precision and unstable performance.

In order to solve the problem of dynamic landmarks, a robust visual-inertial motion prior SLAM system is proposed in this paper which is applicable to a large range of dynamic environments and only uses the motion prior propagated by the IMU in a short period of time to process dynamic landmarks. This paper presents our work from the following aspects:

(1) **The preprocessing of potential dynamic landmarks with inertial motion prior:** The minimum projection errors of landmarks are obtained from inertial motion prior and epipolar constraint to eliminate dynamic landmarks that significantly deviate from the motion prior and mark dynamic candidate landmarks during the feature tracking phase.

(2) **The bundle adjustment (BA) residual for dynamic candidate landmarks:** A dynamic visual residual is constructed which is used in nonlinear optimization process based on sliding window to reduce the impact of landmarks that deviate from the motion prior.

Compared with existing methods in the VIODE dataset [8] which contains dynamic objects within different ranges, superior robust and stable localization accuracy, and good real-time performance of our approach are demonstrated. In addition, the localization accuracy is compared in the EUROC dataset [9], and the result demonstrates stable and superior performance of our approach in static environments.

II. RELATED WORK

VI-SLAM algorithms utilize the inertial measurement unit to correct the scale and the camera poses while V-SLAM algorithms only use visual sensors. Generally, they can be divided into filter-based methods and optimization-based methods which have become mainstream. For example, the ROVIO [10] employed the extended Kalman filter (EKF) method, while OKVIS [11] proposed a keyframe-based framework using optimization process. The ORB descriptor [12] for feature matching was employed to optimize camera poses and landmark positions with IMU measurements in ORB-SLAM3 [13]. The VINS-Fusion [14] is an extended version of VINS-Mono [15], which supports stereo cameras with IMU and adopts feature tracking instead of descriptor matching. However, the above VI-SLAM methods still have

¹Weilong Sun, ²Yumin Zhang and ²Boren Wei are with the College of Instrumental Science and Optoelectronic Engineering, Beijing University of Aeronautics and Astronautics, Beijing 100191, China.

* Corresponding author: Prof. Yumin Zhang.

This research would like to thank colleges of the MGNC Lab., Beijing University of Aeronautics and Astronautics and Prof. Wei Sheng for useful discussions.

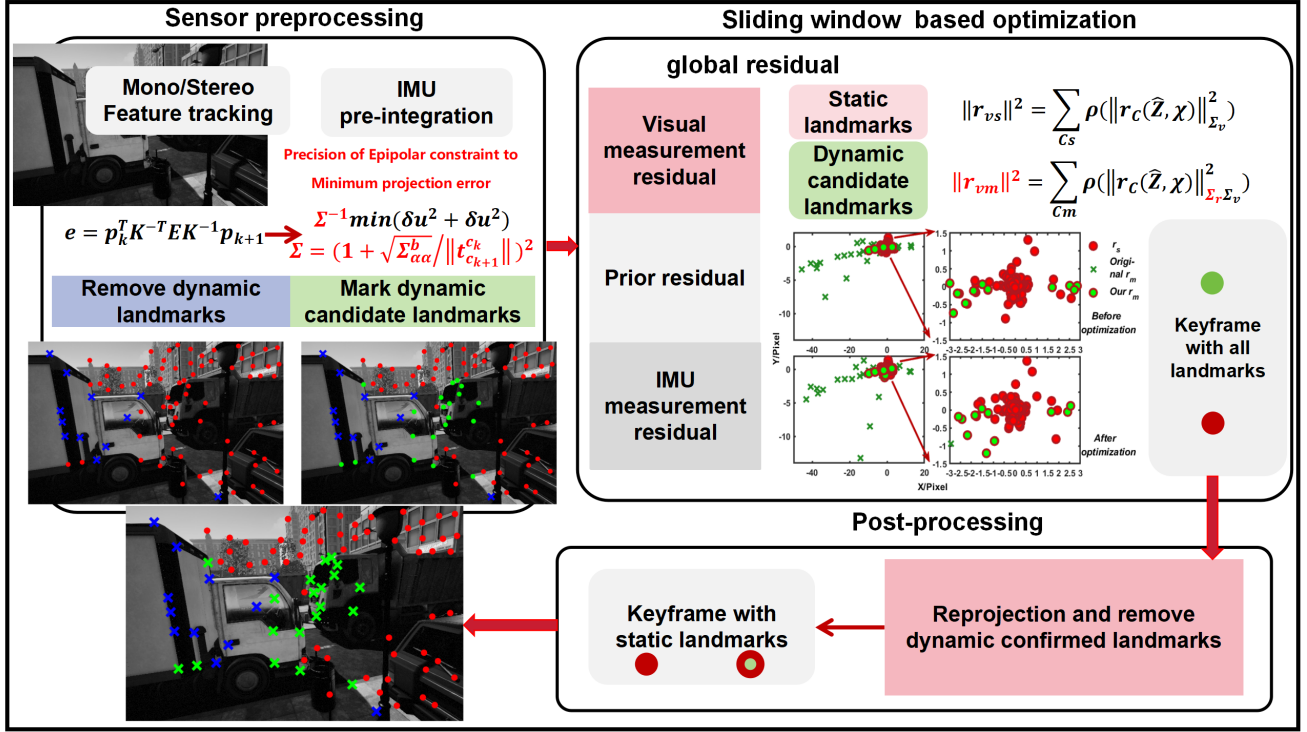


Fig. 1: **System overview:** Our system consists of two main components: (1) Sensor preprocessing, which gets landmarks' minimum projection errors from inertial motion prior and epipolar constraint to eliminates dynamic landmarks and mark dynamic candidate landmarks; (2) Sliding window based optimization with bundle adjustment residual for dynamic candidate landmarks, which minimizes the impact of dynamic candidate landmarks that deviate from the motion prior. And the post-processing component, which removes confirmed dynamic landmarks from sliding window.

potential limitations in dealing with dominant dynamic objects.

Recently, many researchers have proposed a variety of methods for dealing with dynamic objects in the V-SLAM and VI-SLAM algorithms.

A. Methods based on vision geometry

Fan et al. [16] proposed a multi-view geometry-based method using RGB-D camera. The type of each landmark is determined to be dynamic or static according to the geometric relationship between the camera motion and the landmark's states after obtaining the camera pose by minimizing the reprojection error. The RANSAC method [17], [18] can also be used to remove dynamic landmarks in small-scale dynamic scenes. In fact, it can distinguish between inliers and outliers in various anomalies such as noise, occlusion and dynamic objects, improving the robustness of model parameter estimation. The multi-view geometry-based methods assume that the camera pose estimation is accurate enough, which will lead to the failure of the algorithms when the estimation is inaccurate due to the presence of too many dynamic objects.

B. Methods based on deep learning

In DynaSLAM [19], the dynamic landmarks in masked areas where predefined dynamic objects by deep learning

networks are removed, while the types of remaining landmarks are determined through multi-view geometry. Wen et al. [20] proposed a method that combines semantic segmentation information and spatial motion information of associated pixels to deal with dynamic objects. Masoud S. Bahraini et al. [21] adopted a method that combines multi-level RANSAC operators with deep learning to distinguish between dynamic landmarks and static landmarks. Although deep learning methods can successfully eliminate the landmarks of dynamic objects, there are still some problems, such as: many methods require predefined dynamic objects; when only a part of a dynamic object can be seen due to occlusion, it may not be detected; the detected dynamic objects may not be in movement but are temporarily stationary.

C. Methods based on inertial sensor

Cui et al. [22] detected and removed dynamic landmarks according to the epipolar constraint provided by the prior of IMU pre-integration, and conducted states estimation by utilizing more accurate static landmarks. The DynaVINS [23] proposed a robust bundle adjustment system based on the IMU pre-integration regularization factor and the weight momentum factor to reject dynamic landmarks. The method in this paper is also based on the motion prior propagated by the IMU which is used to label potential dynamic landmarks, and we propose a robust bundle adjustment residual for dynamic candidate landmarks.

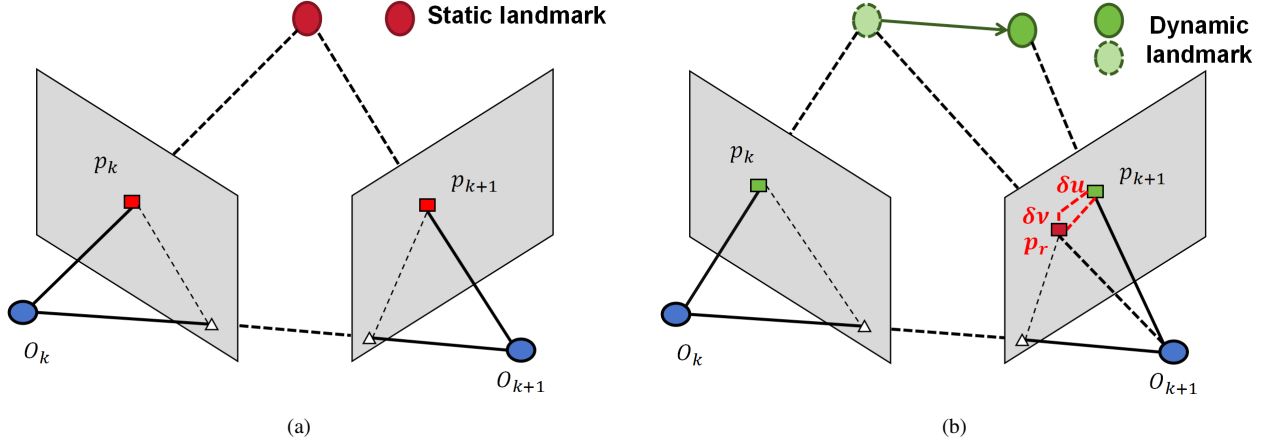


Fig. 2: **The epipolar constraint of landmarks:** The epipolar constraint precision of landmarks between k th frame and $(k+1)$ th frame should approach to zero for (a): static landmark and deviate from zero for (b): dynamic landmark.

III. PREPROCESSING

In this section, the method for preprocessing potential dynamic landmarks with inertial motion prior is introduced. Due to the IMU propagation motion prior between two frames of camera, the minimum projection error is obtained through the landmark's precision of the epipolar constraint, then its probability model is modeled and applied to determine dynamic landmarks will be eliminated and dynamic candidate landmarks will be marked during the tracking phase.

A. Inertial Motion Prior

The relative translation and rotation in the camera coordinate system can be calculated by IMU propagation result and the extrinsic parameters between IMU and camera. The residual covariance matrix of IMU pre-integration [24] can be linearly propagated with the first-order approximation, it will be recursively obtained from the initial covariance $\Sigma_{b_k}^{b_k} = 0$ and the diagonal covariance of noise Q .

$$\left\{ \begin{array}{l} R_{c_{k+1}}^{c_k} = R_c^{b_{k+1}^{-1}} \cdot R_{b_{k+1}}^{b_k} \cdot R_c^b \quad (a) \\ t_{c_{k+1}}^{c_k} = R_c^{b_{k+1}^{-1}} \cdot (P_{b_{k+1}}^{b_k} - t_c^b) \quad (b) \\ \Sigma_{i+1}^{b_k} = (I + F_i \Delta t_i) \Sigma_i^{b_k} (I + F_i \Delta t_i)^T \\ \quad + (G_i \Delta t_i) Q (G_i \Delta t_i)^T \quad (c) \end{array} \right. \quad (1)$$

$[R_c^b, t_c^b]$ represents the extrinsic parameters, $P_{b_{k+1}}^{b_k}$ and $R_{b_{k+1}}^{b_k}$ respectively are the translation vector and rotation matrix obtained from the propagation in the IMU coordinate system, b denotes the IMU coordinate system while c denotes the camera coordinate system. $i \in [k, k+1]$ represents the IMU between two frames of camera, and $[F_i, G_i]$ is the partial derivative of the residual term and the noise term when the residual is expanded by the first-order Taylor series.

B. Minimum Projection Error and Preprocessing

Considering the epipolar constraint and the projection relationship of the landmarks between two frames of camera as **Fig.2**, and under the influence of the two-dimensions' projection residual, the precision of the epipolar constraint is not exactly zero.

$$\begin{aligned} e &= x_k^T \left(t_{c_{k+1}}^{c_k} \right)^\wedge R_{c_{k+1}}^{c_k} x_{k+1} \\ &= p_k^T K^{-T} \left(t_{c_{k+1}}^{c_k} \right)^\wedge R_{c_{k+1}}^{c_k} K^{-1} p_{k+1} \\ &= [a, b, c] \cdot \begin{bmatrix} u_{k+1} \\ v_{k+1} \\ 1 \end{bmatrix} \\ &= [a, b, c] \cdot \begin{bmatrix} u_r + \delta u \\ v_r + \delta v \\ 1 \end{bmatrix} \end{aligned} \quad (2)$$

e represents the precision of the epipolar constraint, $[x_k, x_{k+1}]$ is the coordinate in the normalized camera coordinate system while $[p_k, p_{k+1}]$ is the coordinate in the pixel coordinate system, p_{k+1} is the coordinate measurement combined the true value $[u_r, v_r]^T$ and the residual $[\delta u, \delta v]^T$ as **Fig.2 (b)**, K is the internal parameter matrix of camera.

The minimum value of the square projection error is obtained based on the precision of the epipolar constraint and the residual covariance of IMU pre-integration.

$$\left\{ \begin{array}{l} [a, b, c] \cdot \begin{bmatrix} u_r \\ v_r \\ 1 \end{bmatrix} = 0, [a, b, c] \cdot \begin{bmatrix} \delta u \\ \delta v \\ 0 \end{bmatrix} = e \quad (a) \\ d_s = \Sigma^{-1} \min (\delta u^2 + \delta v^2) = \Sigma^{-1} \cdot e^2 / (a^2 + b^2) \quad (b) \\ \Sigma = \left(1 + \sqrt{\Sigma_{\alpha\alpha}^b} / \|t_{c_{k+1}}^{c_k}\| \right)^2 \quad (c) \end{array} \right. \quad (3)$$

d_s is the minimum square projection error defined by us. Σ^{-1} is a factor that characterizes the credibility of the motion

prior obtained through IMU propagation, which is defined to avoid the incorrect elimination of dynamic landmarks caused by large IMU propagation error (mainly considered as translation error) or the degradation of the epipolar constraint due to an overly small translation amount. $\Sigma_{\alpha\alpha}^b$ is the variance of the position error of IMU pre-integration. Noted that for the pinhole camera model, we adopt the projection error on the pixel plane, while for the fisheye camera model, we use the projection unit length error on the normalized plane.

The square root of projection error $||[\delta u, \delta v]^T||$ of landmark tracked between two frames of camera is modeled with a Gaussian distribution. So Σ in (3.c) can be interpreted from the probabilistic perspective as the variance of the Gaussian distribution, $||[\delta u, \delta v]^T|| \sim N(0, \Sigma)$. Then the distribution of d_s will be approximate to a chi-square distribution with one degree of freedom. The expectation of its coefficient of variation (CV) should approach to $\sqrt{2}$. The elimination and marking strategies for potential dynamic landmarks are as follows.

(1) **Elimination in preprocess:** In the situation where both dynamic and static landmarks exist, the value of CV is always greater than $\sqrt{2}$. Sort all landmarks in descending order according to the value of d_s , and start eliminating from the maximum value until the CV no longer decreases or the CV decreases to the target value $\sqrt{2}$. The elimination criterion and the recursive formulas for mean, variance and CV of remaining landmarks are as follows.

$$\begin{cases} (d_s)_n > \lambda_{dy} \text{ and } n \in \ell_{dy}, & \text{dynamic} \\ (d_s)_n \leq \lambda_{dy} \text{ or } n \notin \ell_{dy}, & \text{otherwise} \end{cases} \quad (4)$$

$$\begin{cases} \mu_{n-1} = (n \cdot \mu_n - (d_s)_n) / (n - 1) & \text{(a)} \\ \sigma_{n-1}^2 = n \cdot \sigma_n^2 / (n - 1) - ((d_s)_n - \mu_{n-1})^2 / n & \text{(b)} \\ CV_{n-1} = \sigma_{n-1} / \mu_{n-1} & \text{(c)} \end{cases} \quad (5)$$

ℓ_{dy} is the set of landmarks that satisfy above standard. Noted that we implement a strict elimination criterion in order to prevent excessive elimination, only the landmarks with a minimum projection error greater than $\lambda_{dy} \text{ pixel}^2$ will execute the elimination operation. $[\mu_n, \sigma_n^2]$ is the mean and variance of the remaining n landmarks.

(2) **Marking in preprocess:** Ignoring the influence of large IMU propagation error and the degradation of the epipolar constraint, the remaining landmarks with a minimum projection error $(\Sigma \cdot d_s)$ greater than $\lambda_{dy}^c \text{ pixel}^2$ are marked as dynamic candidate landmarks. During the non-linear optimization process, these landmarks will be treated differently from static landmarks.

$$\begin{cases} (\Sigma \cdot d_s)_n > \lambda_{dy}^c, & \text{dynamic candidate} \\ (\Sigma \cdot d_s)_n \leq \lambda_{dy}^c, & \text{static} \end{cases} \quad (6)$$

(3) **Mask for extracting landmarks:** After elimination and marking, the area within $\sqrt{2d_s} \text{ pixel}$ around the elimi-

nated dynamic landmark is considered the dynamic candidate area and no new landmarks will be extracted.

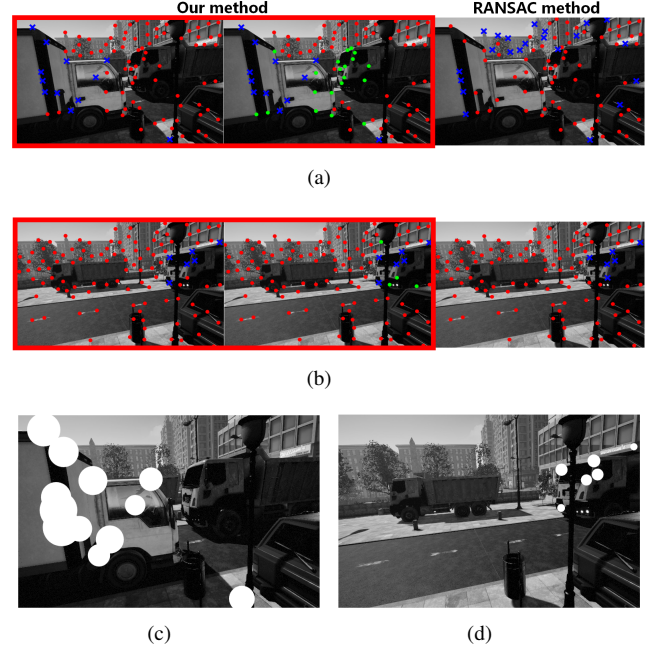


Fig. 3: **Preprocess of dynamic landmarks:** Eliminate dynamic landmarks that significantly deviate from the inertial motion prior and mark dynamic candidate landmarks during the feature tracking phase. The blue \times marks the rejected dynamic landmarks, the green \bullet marks the dynamic candidate landmarks, and the red \bullet marks the static landmarks. (a): The effect comparison of our method and the RANSAC method on the frame with large-scale dynamic objects; (b): The comparison on the frame with small-scale dynamic objects. (c) and (d): The white masks are the dynamic candidate areas where no new landmarks will be extracted for next feature tracking process.

IV. ROBUST BUNDLE ADJUSTMENT

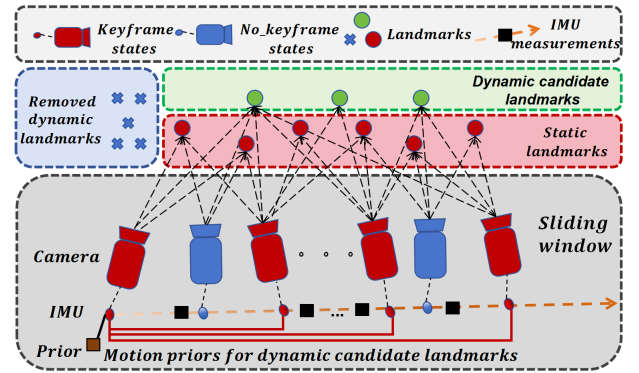


Fig. 4: **Sliding window contains static and dynamic candidate landmarks:** The marked dynamic candidate landmarks in the feature tracking phase are treated differently from the static landmarks in the sliding window.

After removing dynamic landmarks and marking dynamic candidate landmarks, tightly coupled [25], high-precision and robust estimation for the camera poses, landmarks and IMU states in the nonlinear optimization process based on sliding window [15] is executed with the goal of minimizing a global residual. And the visual residual for dynamic candidate landmarks is proposed in this paper to further reduce the influence of them on the optimization results considering the role of kernel function.

When a dynamic candidate landmark enters the sliding window based optimization process, it is continuously observed for n times. The visual residual for these observations is as (7.a) which considers the prior of minimum projection error which will also be updated during the iterative optimization process. From the probabilistic perspective, the two-dimensions' projection residual of dynamic candidate landmarks satisfies a Gaussian distribution with a covariance matrix of minimum value as (7.c).

$$\left\{ \begin{array}{l} \|r_{vm}\|^2 = \sum_{(m,j) \in C_m} \rho \left(\|r_C(\hat{Z}_m^{c_j}, \chi)\|_{\Sigma_r \Sigma_v}^2 \right) \quad (a) \\ \rho(s) = \begin{cases} s, & s < 1 \\ 2\sqrt{s} - 1, & s \geq 1 \end{cases} \quad (b) \\ \Sigma_r = \begin{bmatrix} \min(\delta u_j^2 + \delta v_j^2) & 0 \\ 0 & \min(\delta u_j^2 + \delta v_j^2) \end{bmatrix} \quad (c) \end{array} \right\} \quad (7)$$

C_m represents the collection of dynamic candidate landmarks in the sliding window, $\hat{Z}_m^{c_j}$ represents the j th observation to landmark m , χ represents the camera pose state, IMU state and landmarks state that are to be optimized, and Σ_r^{-1} is the reduction factor of dynamic candidate landmarks' visual residuals, and it is related to the prior of minimum projection error (more than one $pixel^2$) obtained through the epipolar constraint precision between the first observation and the j th ($j \in [2, 3, \dots, n]$) observation in the sliding window. ρ is huber kernel function [26]. Noted that $\|*\|_{\Sigma}^2 = (*)^T \Sigma^{-1} (*)$.

Combined with the visual residuals of static landmarks, the measurement residuals of the IMU and the prior residual, the global residual to be minimized is (8).

$$\begin{aligned} \min_{\chi} & \left\{ \|r_p - H_p \chi\|^2 + \sum_{k \in B} \|r_B(\hat{Z}_{b_{k+1}}^{b_k}, \chi)\|_{\Sigma_{b_{k+1}}^{b_k}}^2 \right. \\ & + \sum_{(s,j) \in C_s} \rho \left(\|r_C(\hat{Z}_s^{c_j}, \chi)\|_{\Sigma_v}^2 \right) \\ & \left. + \sum_{(m,j) \in C_m} \rho \left(\|r_C(\hat{Z}_m^{c_j}, \chi)\|_{\Sigma_r \Sigma_v}^2 \right) \right\} \quad (8) \end{aligned}$$

C_s is the collection of static landmarks in the sliding window, and Σ_v is the covariance matrix of static landmark's projection residual. B represents the collection of inertial measurements while $\Sigma_{b_{k+1}}^{b_k}$ is the residual covariance matrix of the IMU pre-integration [24] between the k th and $(k+1)$ th frames. $[r_p, H_p]$ represents prior information.

After optimization, 3D-2D projection from the first observation to other relevant observations is performed to calculate

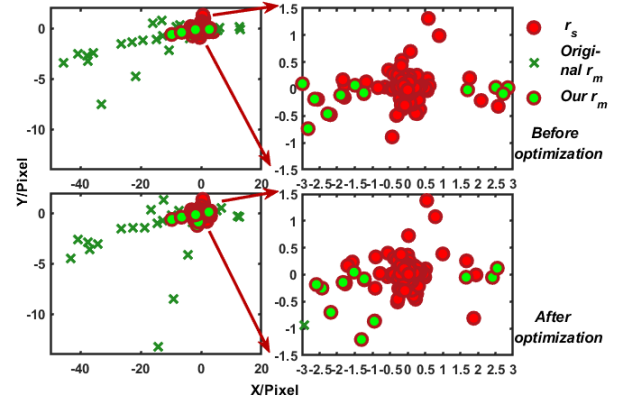


Fig. 5: **Comparison between our residuals and original residuals of landmarks:** r_s represents residual of static landmarks while r_m represents residual of dynamic candidate landmarks, original global visual residual considering huber kernel function is **352.22 $pixel^2$** before optimization and **324.73 $pixel^2$** after optimization, while our is **154.74 $pixel^2$** and **141.85 $pixel^2$** respectively.

the reprojection errors of dynamic candidate landmarks. Remove them outside the sliding window and mark them as confirmed dynamic landmarks if the errors are still relatively large.

V. EXPERIMENTAL RESULTS

To evaluate our proposed algorithm, comparisons with the SOTA algorithms in the VIODE and EUROC datasets are carried out, such as VINS-FUSION [14], VINS-FUSION_ransac and Dyna-VINS [23] in the stereo mode.

A. Datasets

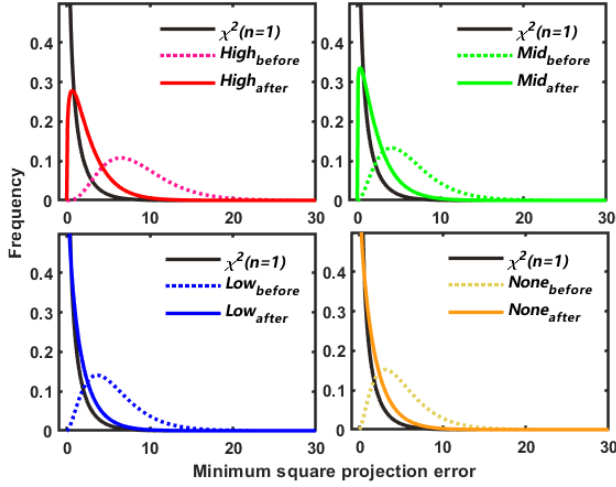
VIODE: VIODE dataset [8] is a simulated dataset that contains lots of dynamic objects, such as cars and trucks. In addition, the dataset includes general occlusion situations. Note that the sub-sequence name none to high means the number and visual field of dynamic objects in the scene.

EUROC: EUROC dataset [9] contains different indoor and factory scenes in the real world. There are no dynamic objects but light intensity changes and violent shakings in it. It is used as a verification that our algorithm remains robust for static environments.

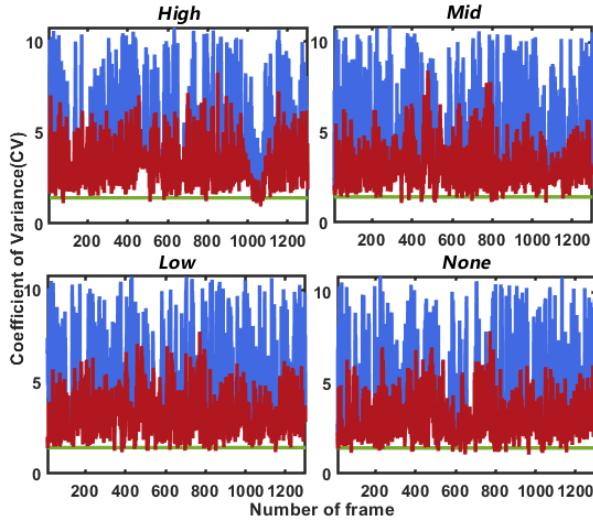
B. Remove dynamic landmarks

After preprocessing to all landmarks during the feature tracking phase, the probabilistic model of landmarks' minimum projection errors is closer to the chi-square distribution with one degree of freedom, and the coefficient of variation (CV) in every frame approaches to $\sqrt{2}$, as Fig.6 in VIODE dataset of day sequences from high to none. λ_{dy} is set to be **4** and λ_{dy}^c is set to be **1** in experiments.

After optimization based on sliding window using our visual residual for dynamic candidate landmarks and post-processing to them, confirmed dynamic landmarks will be removed from sliding window while others will be marked



(a) Fitted probability density curve



(b) Coefficient of variation

Fig. 6: **Remove dynamic landmarks in preprocess of VIODE day sequences:** (a) : Fitted probability density curve for minimum projection error of sequences from day_high to day_none, and the comparison before and after elimination; (b) Coefficient of variation for every frame, blue and red respectively represent CV before and after elimination.

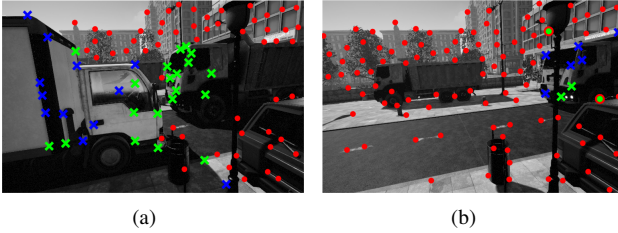


Fig. 7: **Post-process of dynamic landmarks:** The green \times marks the confirmed dynamic landmarks, the green \bullet in red \circ marks the confirmed static landmarks.

as static landmarks. The reduced dynamic visual residual result compared with original residual is displayed in **Fig.5** and final labels of landmarks in **Fig.3** is displayed in **Fig.7**.

C. Qualitative Analyses

This subsection provides a quantitative analysis of our method, evaluating the localization accuracy of camera poses and the time taken. Tables I and II present the comparison of our proposed method with other state-of-the-art SLAM methods, using the RMSE (Root Mean Square Error) of ATE (Absolute Trajectory Error) and average tracking and optimization time cost as the evaluation metric. To comprehensively validate the fitness for environments within different dynamic ranges and the effectiveness of the proposed method, we conducted tests on the VIODE dynamic dataset and the EUROC static dataset.

The effects of the proposed method on the localization accuracy is analyzed as shown in Table I. And Table II shows the analysis of our method on the tracking and optimization time cost. The comparison of the trajectory results in the $[x, y]^T$ directions for different methods and ground truth are shown in **Fig.8**.

(1) The improvement of localization accuracy for different environments: According to Table I, our method has a better result than VINS-Fusion and Dyna-VINS while the RANSAC method has the problem of erroneously removing static inliers when facing large-scale dynamic scenes, like **Fig.3(a)**, which leads to the decline and instability of the accuracy, although the RANSAC method can achieve good results in some cases. For outdoor sequences of VIODE from day_none to day_high, our method improves the localization accuracy by **6.3%**, **14.2%**, **30.1%** and **40.3%** compared to VINS-Fusion. And our method improves the localization accuracy by **10.7%**, **29.4%**, **25.5%** and **47.0%** compared to VINS-Fusion for indoor parking lot sequences of VIODE from parking_lot_none to parking_lot_high. The results of EUROC sequences in real world prove that our method still has a stable improvement effect on the localization accuracy in static environments. Although in some cases, the improvement effect is not as good as RANSAC method for EUROC dataset, but it is better than Dyna-VINS method. Moreover, the performance of Dyna-VINS method is related to complex parameters.

(2) Better time cost performance: According to Table II, our method does not cause too much additional tracking time cost compared to RANSAC method. However, it should be noted that the time consumption will surely be higher than VINS-Fusion and Dyna-VINS which do not conduct additional elimination operations during the feature tracking phase. On the other hand, the optimized results converge more quickly for our method than VINS-Fusion and VINS-Fusion_ransac methods because of the elimination of obvious dynamic landmarks during feature tracking and the classification of dynamic candidate landmarks and static landmarks during optimization process. And the more dynamic objects there are in the environment, the better improvement on the consumption of optimization time will be for our method,

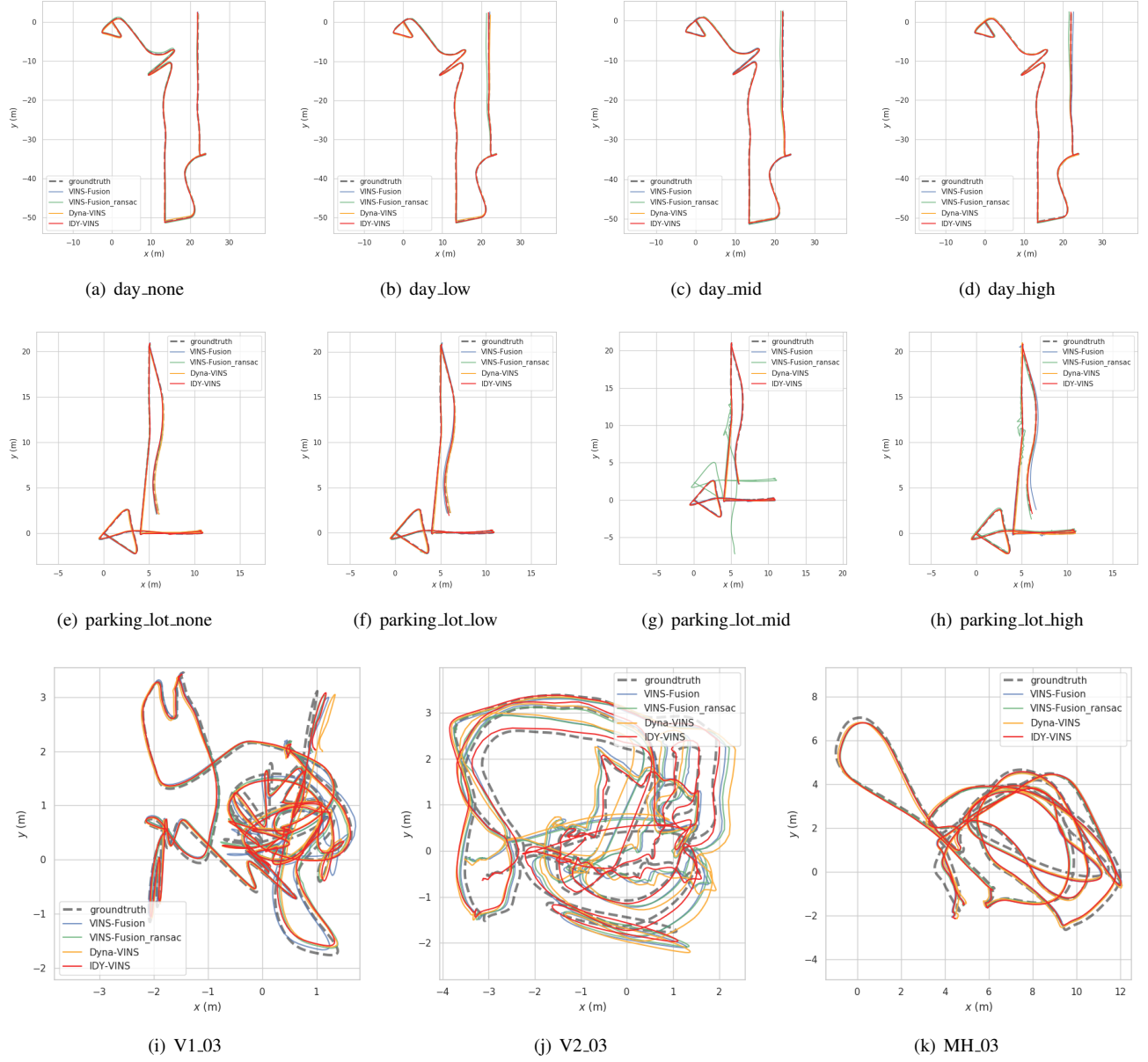


Fig. 8: Comparison of the trajectory results in the $[x, y]^T$ directions for different methods and ground truth.

Table I Comparison of Localization accuracy with state-of-the-art methods (RMSE of ATE in [m]). Noted that x represents failure case (diverged).

Method	VIODE city				VIODE parking_lot				EUROC		
	none	low	mid	high	none	low	mid	high	V1.03	V2.03	MH.03
VINS-Fusion	0.158	0.169	0.193	0.211	0.103	0.126	0.149	0.166	0.216	0.352	0.290
VINS-Fusion_ransac	0.318	0.289	0.298	0.301	0.099	0.097	x	0.310	0.109	0.370	0.266
Dyna-VINS	0.157	0.140	0.149	0.122	0.115	0.099	0.126	0.124	0.175	0.479	0.349
IDY-VINS	0.148	0.145	0.135	0.126	0.092	0.089	0.111	0.088	0.143	0.229	0.276

Table II Time cost experiment tested in day sequences of VIODE dataset from none to high. Noted that the max number of landmarks every frame is set to 120.

Method	Average tracking time cost (ms)				Average optimization time cost (ms)			
	day_none	day_low	day_mid	day_high	day_none	day_low	day_mid	day_high
VINS-Fusion	19.562	20.671	20.473	19.568	39.565	38.894	39.245	37.642
VINS-Fusion_ransac	19.621	21.704	21.752	22.155	38.393	38.984	39.848	38.887
Dyna-VINS	19.353	19.504	19.498	19.703	55.755	48.155	43.628	49.859
IDY-VINS	20.403	20.759	20.628	20.908	38.375	37.375	37.251	35.564

while the RANSAC method often requires a longer optimization time to achieve convergence with a lower localization accuracy because of incorrect elimination. Meanwhile, DynaVINS method requires much more time for optimization due to its complex processing. The above two aspects of tracking time cost and optimization time cost demonstrate that our method generally has a better real-time performance.

VI. CONCLUSIONS

In this paper, the robust visual-inertial motion prior SLAM system (*IDY-VINS*) has been proposed, which effectively handles dynamic landmarks using inertial motion prior for dynamic environments to varying degrees. It is a robust system that preprocesses potential dynamic landmarks and constructs bundle adjustment (BA) residual for dynamic candidate landmarks to reduce their impact. Experimental evidences demonstrate that our algorithm has a superior performance compared to other algorithms in both simulated and real environments, both dynamic and static environments.

In future work, we plan to extend the consideration of dynamic landmarks and candidate landmarks to the overall relocalization and loop closure detection processes of VI-SLAM.

REFERENCES

- [1] Liangyu Zhao, Yeqing Zhu, and Rui Jin. Influence of review of monocular v-slam for multi-rotor unmanned aerial vehicle. *Aero Weaponry*, 27(2):1–14, 2020.
- [2] Jianjun Gui, Dongbing Gu, Sen Wang, and Huosheng Hu. A review of visual inertial odometry from filtering and optimisation perspectives. *Advanced Robotics*, 29(20):1289–1301, 2015.
- [3] Ao Li, Jikai Wang, Meng Xu, and Zonghai Chen. Dp-slam: A visual slam with moving probability towards dynamic environments. *Information Sciences*, 556:128–142, 2021.
- [4] Jonathan Long, Evan Shelhamer, and Trevor Darrell. Fully convolutional networks for semantic segmentation. In *Proceedings of the IEEE conference on computer vision and pattern recognition*, pages 3431–3440, 2015.
- [5] Vijay Badrinarayanan, Alex Kendall, and Roberto Cipolla. Segnet: A deep convolutional encoder-decoder architecture for image segmentation. *IEEE transactions on pattern analysis and machine intelligence*, 39(12):2481–2495, 2017.
- [6] Richard Hartley and Andrew Zisserman. *Multiple view geometry in computer vision*. Cambridge university press, 2003.
- [7] H Christopher Longuet-Higgins. A computer algorithm for reconstructing a scene from two projections. *Nature*, 293(5828):133–135, 1981.
- [8] Koji Minoda, Fabian Schilling, Valentin Wüest, Dario Floreano, and Takehisa Yairi. Viode: A simulated dataset to address the challenges of visual-inertial odometry in dynamic environments. *IEEE Robotics and Automation Letters*, 6(2):1343–1350, 2021.
- [9] Michael Burri, Janosch Nikolic, Pascal Gohl, Thomas Schneider, Joern Rehder, Sammy Omari, Markus W Achtelik, and Roland Siegwart. The euroc micro aerial vehicle datasets. *The International Journal of Robotics Research*, 35(10):1157–1163, 2016.
- [10] Michael Bloesch, Sammy Omari, Marco Hutter, and Roland Siegwart. Robust visual inertial odometry using a direct ekf-based approach. In *2015 IEEE/RSJ international conference on intelligent robots and systems (IROS)*, pages 298–304. IEEE, 2015.
- [11] Stefan Leutenegger, Simon Lynen, Michael Bosse, Roland Siegwart, and Paul Furgale. Keyframe-based visual-inertial odometry using non-linear optimization. *The International Journal of Robotics Research*, 34(3):314–334, 2015.
- [12] Raul Mur-Artal, Jose Maria Martinez Montiel, and Juan D Tardos. Orb-slam: a versatile and accurate monocular slam system. *IEEE transactions on robotics*, 31(5):1147–1163, 2015.
- [13] Carlos Campos, Richard Elvira, Juan J Gómez Rodríguez, José MM Montiel, and Juan D Tardós. Orb-slam3: An accurate open-source library for visual, visual-inertial, and multimap slam. *IEEE Transactions on Robotics*, 37(6):1874–1890, 2021.
- [14] Tong Qin, Shaozu Cao, Jie Pan, and Shaojie Shen. A general optimization-based framework for global pose estimation with multiple sensors. *arXiv preprint arXiv:1901.03642*, 2019.
- [15] Tong Qin, Peiliang Li, and Shaojie Shen. Vins-mono: A robust and versatile monocular visual-inertial state estimator. *IEEE transactions on robotics*, 34(4):1004–1020, 2018.
- [16] Yingchun Fan, Hong Han, Yuliang Tang, and Tao Zhi. Dynamic objects elimination in slam based on image fusion. *Pattern Recognition Letters*, 127:191–201, 2019.
- [17] Rahul Raguram, Jan-Michael Frahm, and Marc Pollefeys. A comparative analysis of ransac techniques leading to adaptive real-time random sample consensus. In *Computer Vision—ECCV 2008: 10th European Conference on Computer Vision, Marseille, France, October 12–18, 2008, Proceedings, Part II 10*, pages 500–513. Springer, 2008.
- [18] David Nistér. Preemptive ransac for live structure and motion estimation. *Machine Vision and Applications*, 16(5):321–329, 2005.
- [19] Berta Bescos, José M Fàcil, Javier Civera, and José Neira. Dynaslam: Tracking, mapping, and inpainting in dynamic scenes. *IEEE Robotics and Automation Letters*, 3(4):4076–4083, 2018.
- [20] Shuhuan Wen, Xiongfei Li, Xin Liu, Jiaqi Li, Sheng Tao, Yidan Long, and Tony Qiu. Dynamic slam: A visual slam in outdoor dynamic scenes. *IEEE Transactions on Instrumentation and Measurement*, 2023.
- [21] Masoud S Bahraini, Ahmad B Rad, and Mohammad Bozorg. Slam in dynamic environments: A deep learning approach for moving object tracking using ml-ransac algorithm. *Sensors*, 19(17):3699, 2019.
- [22] Linfei Cui and Dandan Huang. Visual inertial slam algorithm for dynamic environments. *Computer Engineering and Design*, (043-003), 2022.
- [23] Seungwon Song, Hyungtae Lim, Alex Junho Lee, and Hyun Myung. Dynavins: a visual-inertial slam for dynamic environments. *IEEE Robotics and Automation Letters*, 7(4):11523–11530, 2022.
- [24] Todd Lupton and Salah Sukkarieh. Visual-inertial-aided navigation for high-dynamic motion in built environments without initial conditions. *IEEE Transactions on Robotics*, 28(1):61–76, 2011.
- [25] Agostino Martinelli. Closed-form solution of visual-inertial structure from motion. *International journal of computer vision*, 106(2):138–152, 2014.
- [26] Peter J Huber. Robust estimation of a location parameter. In *Breakthroughs in statistics: Methodology and distribution*, pages 492–518. Springer, 1992.